

# Journal of Materials Chemistry A

Accepted Manuscript



This is an *Accepted Manuscript*, which has been through the Royal Society of Chemistry peer review process and has been accepted for publication.

*Accepted Manuscripts* are published online shortly after acceptance, before technical editing, formatting and proof reading. Using this free service, authors can make their results available to the community, in citable form, before we publish the edited article. We will replace this *Accepted Manuscript* with the edited and formatted *Advance Article* as soon as it is available.

You can find more information about *Accepted Manuscripts* in the [Information for Authors](#).

Please note that technical editing may introduce minor changes to the text and/or graphics, which may alter content. The journal's standard [Terms & Conditions](#) and the [Ethical guidelines](#) still apply. In no event shall the Royal Society of Chemistry be held responsible for any errors or omissions in this *Accepted Manuscript* or any consequences arising from the use of any information it contains.



## High performance carbon nanotube based fiber-shaped supercapacitors using redox additives of polypyrrole and hydroquinone

Received 00th January 20xx,  
Accepted 00th January 20xx

DOI: 10.1039/x0xx00000x

www.rsc.org/Materials A

Ruiqiao Xu, Fengmei Guo, Xian Cui, Li Zhang, Kunlin Wang and Jinquan Wei\*

Fiber-shaped supercapacitors (FSSCs) have attractive applications in the flexible devices. Here, we report a high performance carbon nanotube (CNT) based fiber-shaped supercapacitor by adding two redox additives simultaneously: polypyrrole (PPy) to the electrodes and hydroquinone (HQ) to the electrolyte. A core-shell CNT-PPy nanocomposite fiber was prepared by an electrochemical deposition method. In the FSSC with CNT-PPy electrodes, PPy provides pseudocapacitance for its reversible dropping/de-dropping reactions in polyvinyl alcohol (PVA)/H<sub>2</sub>SO<sub>4</sub> gel electrolyte. The capacitance of the CNT-PPy FSSC reaches 36 F/g (127 mF/cm, 588 mF/cm<sup>2</sup>, 17 F/cm<sup>3</sup>), which is 7 times higher than that of the pure CNT FSSC. By adding HQ to the PVA/H<sub>2</sub>SO<sub>4</sub> gel electrolyte in the CNT-PPy FSSC, the specific capacitance reaches 56 F/g (202 mF/cm, 1168 mF/cm<sup>2</sup>, 42 F/cm<sup>3</sup>), which is 10 times higher than that of the pure CNT FSSC. HQ can enhance ion transfer of the gel electrolyte by the redox reaction of HQ and benzoquinone. PPy and HQ have synergistic effects in the FSSCs. The FSSCs with PPy and HQ also show high stability in the cyclic test for 2000 cycles, and good flexibility under bending, knotting, and suffering tension.

### 1. Introduction

As a new kind of flexible, lightweight, and high power energy storage device, fiber-shaped supercapacitor (FSSC) has attracted tremendous interests due to its potential applications in wearable smart clothes and flexible electronics.<sup>1</sup> Carbon nanotubes (CNTs) have been widely used as efficient fiber electrodes owing to their superior properties, such as high electrical conductivity, abundant porous structure, outstanding mechanical properties, high chemical stability, and well-established fabrication technology.<sup>2-4</sup> However, the FSSCs using the pure CNTs as electrodes usually have relatively low specific capacitance and energy density, due to operating under the electrochemical double-layered capacitor mechanism. A common strategy to improve the capacitance of FSSCs is to introduce pseudocapacitive materials to electrodes, such as MnO<sub>2</sub><sup>5,6</sup>, PPy<sup>7</sup>, PANI<sup>8</sup>, PEDOT<sup>9</sup>, and so on. Among these additives, polypyrrole (PPy) is one of the best candidates due to its high faradic activity, good electrical conductivity, low-cost, and environmental friendship.<sup>10</sup>

Recently, a new strategy to improve the performance of the supercapacitors has been reported by introducing single or double redox additives (such as KI<sup>11</sup>, VOSO<sub>4</sub><sup>12</sup>, methylene

blue<sup>13</sup>) into liquid or gel electrolyte. Pan et al.<sup>14</sup> introduced redox-active 2-mercaptopyridine (PySH) into polyvinyl alcohol (PVA)/H<sub>2</sub>SO<sub>4</sub> gel electrolyte and attained a FSSC with a high areal capacitance of 507 mF/cm<sup>2</sup>. Hydroquinone (HQ) can store electrons at electrode/electrolyte interfaces when it is oxidized into benzoquinone (BQ), which has also been used to enhance capacitance of double-layer supercapacitors.<sup>15, 16</sup> Vonlanthen et al.<sup>17</sup> fabricated a liquid-state supercapacitor with a high pseudocapacitance by using PANI-Pt electrodes and HQ added H<sub>2</sub>SO<sub>4</sub> aqueous electrolyte. However, to our best knowledge, few research focused on all-solid-state FSSCs using redox additives in electrode and electrolyte at the same time.

Here, we report a high performance all-solid-state CNT-based FSSC by using two redox additives simultaneously: PPy in electrodes and HQ in electrolyte. Due to synergistic effects between PPy and HQ, the FSSC achieves a specific capacitance of 55.7 F/g (0.2 F/cm, 1.2 F/cm<sup>2</sup>, 42.5 F/cm<sup>3</sup>). The FSSC also shows high cyclic stability with ~103 % capacitance retention after 2000 cycles and good flexibility under bending, knotting and suffering tension.

### 2. Experimental

#### Preparation of fiber electrodes

The CNT macroscopic films were directly fabricated using an improved floating chemical deposition method.<sup>18, 19</sup> The as-prepared CNT films, consisting mainly of single-walled and double-walled CNTs, are about 6 cm in width, 80 cm in length, and tens of

Key Laboratory for Advanced Materials Processing Technology of Education Ministry; State Key Laboratory of New Ceramic and Fine Processing; School of Materials Science and Engineering, Tsinghua University, Beijing 100084, P.R. China  
E-mail: jqwei@tsinghua.edu.cn; Tel: +86-10-62781065

microns in thickness. The as-prepared CNT films were purified by treating in 30% H<sub>2</sub>O<sub>2</sub> for two days and then in 37% HCl for 12 h to remove catalyst particles and amorphous carbon. After purification, the CNT films were cut into strips with dimension of 5 mm×80 mm (See supporting information of Fig. S1a). In order to make a homogeneous nanocomposite, the strips were immersed in a 0.1 M pyrrole aqueous solution for 8 hours to allow pyrrole monomers to fully penetrate the strips. The PPy was then electrochemically deposited onto the CNT strips by a three-electrode system using a CNT strip as working electrode, a saturated calomel electrode (SCE) as reference electrode and a platinum wire as counter electrode (See supporting information of Fig. S1b). A potential of 0.7 V (vs SCE) was applied for 300–600 s in an electrolyte of 0.1 M pyrrole and 0.1 M NaClO<sub>4</sub> aqueous solution. After washing in deionized (DI) water, the CNT-PPy nanocomposite strips were transferred to a glass slide and covered by another. Then, the nanocomposite strips were spun for about 10000 turns per meter into fibers from one side by an electric motor (See supporting information of Fig. S1c). After drying in vacuum at 80 °C for 10 hours, the weights and diameters of the fibers were measured. For comparison, pure CNT fibers were also prepared by spinning from the purified CNT strips.

#### Preparation of gel electrolytes

To prepare gel electrolyte, 1 g PVA and 0.01 mol H<sub>2</sub>SO<sub>4</sub> were dissolved in 10 mL DI water. After magnetically stirring at 90 °C for 30 min, the solution transferred to a transparent PVA/H<sub>2</sub>SO<sub>4</sub> gel electrolyte (See supporting information of Fig. S2a). In order to enhance the electrochemical performance of the gel electrolyte, 0.3 g hydroquinone (HQ) was added into 10 mL PVA/H<sub>2</sub>SO<sub>4</sub> solution followed by stirring at 60 °C for 30 min. After evaporation at room temperature for 2 hours, the transparent gel electrolyte turned to opaque and formed a quasi-solid state (See supporting information of Fig. S2b).

#### Fabrication of fiber-shaped supercapacitors

To prepare symmetric fiber-shaped supercapacitors (FSSCs), two fibers were separately immersed into the as-prepared gel electrolyte for a few minutes, and then dried at room temperature for 2 h to form a homogeneous coating of quasi-solid gel electrolyte. Then, the two fibers were carefully placed in parallel. The gel electrolyte was coated on the two parallel fibers one more time to form an all-solid-state FSSC. We fabricated four kinds of FSSCs by controlling the type of fiber electrodes and electrolyte: pure CNT fiber electrodes, and the gel electrolyte with and without HQ (denoted as CNT-HQ and CNT); CNT-PPy fiber electrodes, and the gel electrolyte with and without HQ (denoted as CNT-PPy-HQ and CNT-PPy), respectively.

#### Characterization

The structure and morphology of the fiber electrodes were characterized by scanning electron microscopy (SEM, LEO 1530) and transmission electron microscopy (TEM, JEOL 2010). Electrochemical tests of the FSSCs were carried out by using a two-electrode system in ambient by an electrochemical workstation (CHI660E, Shanghai Chen Hua Co., Ltd, China). Cyclic voltammetry (CV) tests and galvanostatic charge-discharge (GCD) tests were performed in a voltage window of 0–0.8 V at different scan rates

and current densities, respectively. The electrochemical impedance spectroscopy (EIS) measurements were conducted at a frequency range from 100 kHz to 0.01 Hz with an AC perturbation of 5 mV at open circuit potential. The calculation method of capacitance, energy density and power density are described in details in supporting information.

### 3. Results and discussion

Fig. 1a displays the fabrication process of an FSSC from CNT strips. According to our previous report<sup>20</sup>, PPy is electrochemically deposited on the CNT strip before spinning. It forms a CNT-PPy nanocomposite after PPy deposition, where PPy coating on the CNT bundles continuously and homogeneously. The CNT-PPy nanocomposite strip is transferred to a glass slide and then covered by another. The CNT-PPy strip is spun into a fiber in wet state from one side to the other by a motor. Water inside the strip acts as a lubricant between the strip and the slides, making the strip move easily during spinning. As the motor rotates, the strip near the edge of the top slide is spun into a fiber shape. By moving the top slide slowly, the strip is released gradually and spun into fiber with a final diameter about 300 μm. Actually, this spinning method has been widely used in traditional fiber fabrications, which can be easily scaled up to make long fibers.

Fig. 1b shows a low magnification SEM image of a CNT-PPy fiber. There are lots of spirals on its surface, which derives from the spinning process. The spirals provide large surface for electrolyte. Due to the entangled CNT bundles, there are still abundant micro-pores within the fiber (See Fig. 1c), which allows electrolyte ions to diffuse inside the fiber freely. As the PPy is deposited before the fiber spinning, pyrrole monomers can fully penetrate the CNT strip, leading to a homogeneous distribution of PPy. As shown in Fig. 1d, the CNT-PPy nanocomposite has a core-shell structure, in which the PPy shell coats the CNT core continuously. For an optimized deposition time of 600 s, the PPy shell has a thickness about 10 nm. The content of the PPy in the composite is about 50 wt. %. The CNT-PPy fibers have a high electrical conductivity of about 180 kS/m, which is slightly lower than that of the pure CNT fibers (~230 kS/m) according to our previous report.<sup>20</sup>

Two CNT-PPy electrodes are placed in parallel and coated by a gel electrolyte to assemble an all-solid-state FSSC. The FSSC is flexible and can wrap around a finger easily (Fig. 1e). Fig. 1f shows a cross-sectional SEM image of a CNT-PPy electrode coated by the gel electrolyte with HQ. The gel electrolyte layer on the fiber has a thickness of about 20 μm and has a good interface with the CNT-PPy electrode. Fig. 1g shows a side-viewed SEM image of a CNT-PPy-HQ FSSC. The two parallel fiber electrodes are coated by the gel electrolyte uniformly. The quasi-solid electrolyte coating can prevent the two fibers from short circuit.

We evaluate the electrochemical performance of the CNT FSSC using PVA/H<sub>2</sub>SO<sub>4</sub> gel electrolyte without HQ. Fig. 2a shows the cyclic voltammetry (CV) curves of a CNT FSSC at various scanning rates ranging from 50 mV/s to 200 mV/s. The CV curves show ideal rectangular shapes, indicating a typical

electrical double layer capacitive (EDLC) behavior. The CNT FSSC retains a good performance at high scan rates (e.g. 10 V/s, see supporting information of Fig. S3a) and wide voltage windows (e.g. 1.2 V, see supporting information of Fig. S3b), which derives mainly from the high electrical conductivity of CNT fibers and their stability in gel electrolyte. However, the specific capacitance of the CNT FSSC reaches only 5.2 F/g at a scan rate of 50 mV/s.

In order to improve the specific capacitance of the CNT FSSC, redox additives are added to the electrodes and electrolyte, respectively. The ionic conductivity of the gel electrolyte needs to be improved to enhance the charge transfer between electrodes and electrolyte. HQ can enhance the ion transfer in the gel electrolyte by its redox reactions.<sup>21</sup> Fig. 2b shows the CV curves of a CNT-HQ FSSC using the gel electrolyte with HQ. The CV curves of the CNT-HQ FSSC still have ideal rectangular shapes, which are similar to those in the Fig. 2a. A slight reduction peak at 0.05 V and an oxidation peak near 0 V are identified, which derives from that the redox reactions cannot fully happen in this potential window for this CNT-HQ FSSC.<sup>21</sup> When the voltage is higher than 0.2 V, the CV curves have almost constant charge and discharge currents, indicating excellent EDLC performance of the CNT-HQ FSSC. Thus, the HQ enhances the ion transfer ability and provides small amount of pseudocapacitance in the FSSCs using pure CNT as electrodes. The specific capacitance of the CNT-HQ increases to 8.0 F/g at 50 mV/s.

Fig. 2c shows the CV curves of a CNT-PPy FSSC using the PVA/H<sub>2</sub>SO<sub>4</sub> gel electrolyte without HQ. The CNT-PPy FSSC behaves a typical hybrid supercapacitor performances, which is similar to that reported previously<sup>19</sup>. The hybrid supercapacitor combines the electrical double-layer capacitance from CNTs and the pseudocapacitance from redox-active PPy. The specific capacitance of the CNT-PPy FSSC reaches 36.1 F/g, which is 7 times higher than that of the CNT FSSC.

Since the specific capacitance of the CNT-based FSSCs can be improved significantly by separately adding the redox additives of PPy to electrodes and HQ to electrolyte, it would be interesting to fabricate a CNT-PPy-HQ FSSC by using the two redox additives simultaneously. Fig. 3a shows the CV curves of a CNT-PPy-HQ FSSC at various scan rates of 20 mV/s-200 mV/s. The CV curves are quite different from those of the above three kinds of FSSCs. There are evident redox-peaks in the CV curves. At 50 mV/s, the oxidation peak of HQ→BQ locates at 0.64 V, and reduction peak of BQ→HQ locates at 0.26 V, which are close to those reported previously<sup>17</sup>. The specific capacitance reaches 55.7 F/g, which is 10 times higher than that of the CNT FSSC. The mass of HQ in gel electrolyte is optimized. The gel electrolyte has the highest ionic conductivity of 23.2 mS/cm for adding 0.3 g HQ to 10 mL gel electrolyte, which is twice higher than that of the pure PVA/H<sub>2</sub>SO<sub>4</sub> gel electrolyte (See supporting information of Fig. S4a). The specific capacitance is also the best for this concentration (See supporting information of Fig.S4b). GCD curves of the CNT-PPy-HQ FSSC at various current densities are shown in Fig. 3b. The GCD curves have approximately equal

charging and discharging times, implying a favourable electrochemical reversibility. When the current density decreases, the non-straight sections in GCD curves become more obvious, indicating a more faradaic contribution to the charge accumulation process.<sup>15</sup>

For comparison, the CV curves of the four kinds of FSSCs at 50 mV/s are displayed in Fig. 4a. It is clear that the CNT-PPy-HQ FSSC has the largest enclosed area of the CV curve. The CV curves of the CNT-PPy FSSC with and without HQ happen to overlap with each other at the beginning of charging and discharging processes. This phenomenon is also observed in CV curves of the two FSSCs at 20 mV/s and 100 mV/s but not at 200 mV/s (see supporting information of Fig.S5). It indicates that the PPy mainly contributes pseudocapacitance to the FSSCs with and without HQ in the gel electrolyte at these stages. In the charging process, there is extra pseudocapacitance at the voltage ranging from 0.2 to 0.8 V in the CNT-PPy-HQ FSSC when compared with the CNT-PPy FSSC. The extra pseudocapacitance in the CNT-PPy-HQ is also observed in the discharging process at the voltage ranging from 0.65 V to 0 V. It clearly shows from the large amount extra pseudocapacitance in the CV curves that HQ has synergistic effects with PPy in the CNT-PPy-HQ FSSC.

Fig. 4b shows GCD curves at 0.2 A/g of the four kinds of FSSCs. The discharging times of the FSSCs using electrolyte with HQ are almost twice longer than those of the FSSCs using the electrolyte without HQ. The GCD voltage drop at beginning of discharging represents an internal consumption of an FSSC. The GCD voltage drop of the CNT-HQ FSSC is only 2.2 mV, which is slightly smaller than that of the CNT FSSC (2.4 mV). This indicates that HQ can reduce the internal resistance of the supercapacitor. The discharging time of the CNT FSSC is only about 20 s, while it extends dramatically to 217 s for the CNT-PPy-HQ FSSC. Fig.4c shows the specific capacitances of the four kinds of FSSCs, which are evaluated from GCD tests at 0.2-1.0 A/g. The specific capacitance of the CNT FSSC is 5.2 F/g at 0.2 A/g. When the GCD current density increases to 1 A/g, the capacitance drops by 5.8%, showing a good rate capacity. The capacitance of the CNT-PPy-HQ FSSC reaches 50.1 F/g at 1.0 A/g, which is still 90% capacitance retention. In comparison, we also calculated the specific capacitances of the FSSCs in terms of length, area or volume, as shown in Table S1. The volumic capacitance of the CNT-PPy-HQ FSSC reaches 42.5 F/cm<sup>3</sup>, corresponding to a linear capacitance of 202.0 mF/cm and an areal capacitance of 1168 mF/cm<sup>2</sup>, which are comparable with or higher than those of the FSSCs reported recently (Table S1), such as MnO<sub>2</sub>-CNT//CNT asymmetric FSSC (27.98 mF/cm<sup>2</sup>, 0.261 mF/cm)<sup>5</sup>, CNT/MC FSSC using PVA-H<sub>2</sub>SO<sub>4</sub>-PySH redox-active electrolyte (507 mF/cm<sup>2</sup>)<sup>14</sup>, CNP-CF based asymmetric FSSC (4.6 F/cm<sup>3</sup>)<sup>22</sup>, MnO<sub>2</sub>-PPy-CF//V<sub>2</sub>O<sub>5</sub>-PANI-CF asymmetric FSSC (613 mF/cm<sup>2</sup>)<sup>23</sup>, MnO<sub>2</sub>-RGO-CF//CH-CW asymmetric FSSC (2.54 F/cm<sup>3</sup>, 50.8 mF/cm<sup>2</sup>)<sup>24</sup>, and graphene coaxial FSSC (180 F/g, 4.63 mF/cm<sup>2</sup>)<sup>25</sup>.

Fig. 4d shows the Ragone plots of the FSSCs. The CNT-PPy-HQ FSSC exhibits the highest energy density among the four kinds of FSSCs. The sequence of the energy density from high to low is CNT-PPy-HQ, CNT-PPy, CNT-HQ, and CNT FSSC.

The volumic energy density of the CNT-PPy-HQ FSSC reaches  $3.6 \text{ mWh/cm}^3$  at a power density of  $59 \text{ mW/cm}^3$ , corresponding to an areal energy density of  $98 \text{ mWh/cm}^2$ , a liner energy density of  $17.0 \text{ } \mu\text{Wh/cm}$ , and a specific energy density of  $4.7 \text{ Wh/kg}$ . At an energy density of  $2.9 \text{ mWh/cm}^3$ , the power density reaches  $281 \text{ mW/cm}^3$ , corresponding to an areal power density of  $7.7 \text{ W/cm}^2$ , a liner power density of  $1.3 \text{ mW/cm}$ , and a specific power density of  $368 \text{ W/kg}$ , which are comparable with or higher than those of the recently reported FSSCs<sup>2,5,26-32</sup>.

The EIS analysis is widely used to investigate the mechanism of charge storage for supercapacitors. The four kinds of FSSCs show vertical lines to real axis at low frequency region in the Nyquist plots (Fig.5a), which reveal ideal capacitive behaviors. For the FSSCs using the CNT-PPy nanocomposite electrodes, such as the CNT-PPy and the CNT-PPy-HQ FSSC, there are small deviated lines with slopes near to 1 at middle frequency region (Fig.5b), indicating larger Warburg/diffusion resistances than those of the FSSCs using pure CNT fibers as electrodes. Meanwhile, small semicircles are identified at high frequency region for devices using the electrolyte with HQ, such as the CNT-HQ and the CNT-PPy-HQ FSSCs, indicating charge transfer resistances related to the redox reactions of HQ. The intersection of Nyquist plots with real axis represents an internal resistance of a FSSC, relating to the electrical conductivity of electrodes and ionic conductivity of electrolyte. When HQ is added to the gel electrolyte, the internal resistance decreases (CNT:  $1.03 \text{ } \Omega$  → CNT-HQ:  $0.69 \text{ } \Omega$ , CNT-PPy:  $1.10 \text{ } \Omega$  → CNT-PPy-HQ:  $0.89 \text{ } \Omega$ ), resulting from the improvement of ionic conductivity of electrolyte by HQ. When PPy is applied to electrodes, the internal resistance increases (CNT:  $1.03 \text{ } \Omega$  → CNT-PPy:  $1.10 \text{ } \Omega$ , CNT-HQ:  $0.69 \text{ } \Omega$  → CNT-PPy-HQ:  $0.89 \text{ } \Omega$ ), resulting from the degradation of electrical conductivity of electrodes by PPy.

Fig. 5c shows the frequency dependent impedances of Bode plots. The plots remain at small resistances at high frequency, and show slant lines with slopes of -1 in low frequency, indicating ideal capacitive behaviors of the FSSCs. Fig.5d shows the frequency dependent phase angles of Bode plots. The highest phase angle of CNT-PPy-HQ is  $82.9^\circ$ , which is close to those of the CNT ( $83.5^\circ$ ) and CNT-PPy ( $84.5^\circ$ ) FSSCs, showing the ideal capacitive behaviors at low frequency region further. The knee frequency ( $f_k$ ) could be acquired at phase angle of  $-45^\circ$  (or at the inflection point of frequency dependent impedance plots), from which the relaxation time constant ( $\tau_0$ ) is evaluated by the equation of  $0.5\pi f_k$ . The time constant describes the time needed to charge a supercapacitor, which can be used to characterize the rate capacity. The time constant of the CNT-PPy-HQ FSSC is  $610 \text{ ms}$ , which is shorter than that of the CNT-PPy FSSC ( $896 \text{ ms}$ ), but much longer than that of the CNT-HQ ( $108 \text{ ms}$ ) and CNT FSSCs ( $23 \text{ ms}$ ). The increase of the time constants by introducing PPy are due to an increase of equivalent distributed resistance, which relates to a harder diffusion of ions within the porous electrodes for a smaller pore size. While, the decrease of the time constant by introducing HQ in CNT-PPy-HQ is due to an improvement in ionic conductivity of the gel electrolyte.

The significant improvement of the electrochemical properties of the CNT-PPy-HQ FSSC is attributed to the synergistic effects of the two redox additives of PPy and HQ. Fig. 6 shows a schematic illustration of the discharging process in the CNT-PPy-HQ FSSC. BQ, generated in the charging process, absorbs hydrogen ions and electrons, and is reduced to HQ at the interface of electrolyte/positive electrode. At the interface of negative electrode/electrolyte, PPy de-dropped in charging process is simultaneously dropped by anions in electrolyte again and produces electrons to balance the circuit. These two reactions take place synergistically. In addition, due to the symmetric structure of the FSSCs, both the redox reactions of HQ/BQ and the dropping/de-dropping processes of PPy can take place on the positive and negative electrodes, simultaneously. Furthermore, the CNT-PPy-HQ FSSC shows a relatively low equivalent series resistance (ESR) of  $0.9 \text{ } \Omega$  at  $1 \text{ kHz}$ , which is one order of magnitude lower than that of the CNT/PEDOT/Pt two-ply electrodes ( $8.5 \text{ } \Omega$ )<sup>9</sup>. The core-shell structure of the CNT-PPy nanocomposite minimizes the charge transfer resistance. Besides, HQ improves the ionic conductivity of PVA-based electrolyte significantly.

In addition to the high specific capacitance, the CNT-PPy-HQ FSSC exhibits a good stability in cyclic test. We performed a cyclic test for 2000 cycles at a current density of  $1 \text{ A/g}$ . As shown in Fig. 7a, with the increase of cycle numbers, the capacitance of the CNT-PPy-HQ FSSC decreases in the first  $\sim 500$  cycles and then increases. The FSSC shows 103% capacitance retention after 2000 cycles. The coulombic efficiency maintained at  $\sim 97\%$  during the cyclic test. The inset of Fig. 7a presents the 1000th-1007th GCD cycles. Each charge-discharge cycle finishes in about  $75 \text{ s}$  and exhibits a typical quasi-triangular shape.

As shown in Fig.7b, the CNT-PPy-HQ FSSC also shows high flexibility and stability under a bending test. For comparison, the original CV curves of the FSSC are provided in the supporting information of Fig. S6. After bending to various angles and recovering during the cyclic tests for 100 cycles (See insets of Fig.7b), the CNT-PPy-HQ FSSC still retains more than 90% of its pristine capacitance. The CV curves of the FSSC before knotting and after de-knotting almost overlap with each other, showing good stability under bending and knotting (See Fig.7c). Furthermore, we also tested the stability of the CNT-PPy-HQ FSSCs under suffering tension by hanging different weights. As shown in Fig. 7d, there is no evident difference in the CV curves when the CNT-PPy-HQ FSSC hangs weights ranging from  $50$  to  $200 \text{ g}$ . The FSSCs can be used as energy storable cables to collect wasted energy in cranes, until their performance is improved to a higher level.<sup>33</sup>

#### 4. Conclusions

In summary, we have successfully fabricated a high performance, flexible, all-solid-state, and fiber-shaped supercapacitor from macroscopic CNT films by using two redox additives of PPy and HQ, simultaneously. The specific capacitance of the pure CNT FSSC was improved from  $5.2 \text{ F/g}$  to  $8.0 \text{ F/g}$  by adding HQ in the PVA/ $\text{H}_2\text{SO}_4$  gel electrolyte; and

to 36.1 F/g by forming core-shell nanocomposite electrodes through an electrochemically deposition of PPy. By adding PPy to the electrodes and HQ to the gel electrolyte simultaneously, the CNT-PPy-HQ FSSC has a high specific capacitance of 55.7 F/g (0.2 F/cm, 1.2 F/cm<sup>2</sup>, 42 F/cm<sup>3</sup>), which are more than one order of magnitude higher than those of the CNT FSSC, due to synergetic effects between PPy and HQ. The CNT-PPy-HQ FSSC also shows a high cyclic stability and performs well under bending, knotting, and suffering tension. The CNT-PPy-HQ FSSC has great potential applications in the flexible electronics and energy storage devices.

### Acknowledgements

This work was supported by National Natural Science Foundation of China (51172122) and Shenzhen Jiawei Photovoltaic Lighting Co., Ltd.

### References

- D. S. Yu, Q. Qian, L. Wei, W. Jiang, K. Goh, J. Wei, J. Zhang and Y. Chen, *Chem. Soc. Rev.*, 2015, **44**, 647-662.
- D. S. Yu, K. L. Goh, H. Wang, L. Wei, W. C. Jiang, Q. Zhang, L. M. Dai and Y. Chen, *Nat. Nanotechnol.*, 2014, **9**, 555-562.
- A. B. Dalton, S. Collins, E. Munoz, J. M. Razal, V. H. Ebron, J. P. Ferraris, J. N. Coleman, B. G. Kim and R. H. Baughman, *Nature*, 2003, **423**, 703.
- Z. B. Yang, J. Deng, X. L. Chen, J. Ren and H. S. Peng, *Angew. Chem. Int. Ed.*, 2013, **52**, 13453-13457.
- P. Xu, B. Q. Wei, Z. Y. Cao, J. Zheng, K. Gong, F. Li, J. Y. Yu, Q. W. Li, W. B. Lu, J. H. Byun, B. S. Kim, Y. S. Yan and T. W. Chou, *ACS Nano*, 2015, **9**, 6088-6096.
- C. Choi, J. A. Lee, A. Y. Choi, Y. T. Kim, X. Lepró, M. D. Lima, R. H. Baughman and S. J. Kim, *Adv. Mater.*, 2014, **26**, 2059-2065.
- Y. Y. Shang, C. H. Wang, X. D. He, J. J. Li, Q. Y. Peng, E. Z. Shi, R. G. Wang, S. Y. Du, A. Y. Cao and Y. B. Li, *Nano Energy*, 2015, **12**, 401-409.
- K. Wang, Q. H. Meng, Y. J. Zhang, Z. X. Wei and M. H. Miao, *Adv. Mater.*, 2013, **25**, 1494-1498.
- J. A. Lee, M. K. Shin, S. H. Kim, H. U. Cho, G. M. Spinks, G. G. Wallace, M. D. Lima, X. Lepró, M. E. Kozlov, R. H. Baughman and S. J. Kim, *Nat. Commun.*, 2013, **4**, 1970.
- Y. P. Fang, J. W. Liu, D. J. Yu, J. P. Wicksted, K. Kalkan, C. O. Topal, B. N. Flanders, J. Wu and J. Li, *J. Power Sources*, 2010, **195**, 674-679.
- S. T. Senthilkumar, R. K. Selvan, Y. S. Lee and J. S. Melo, *J. Mater. Chem. A*, 2013, **1**, 1086-1095.
- L. Q. Fan, J. Zhong, J. H. Wu, J. M. Lin and Y. F. Huang, *J. Mater. Chem. A*, 2014, **2**, 9011-9014.
- S. Roldán, M. Granda, R. Menéndez, R. Santamaría and C. Blanco, *Electrochim. Acta*, 2012, **83**, 241-246.
- S. W. Pan, J. Deng, G. Z. Guan, Y. Zhang, P. N. Chen, J. Ren and H. S. Peng, *J. Mater. Chem. A*, 2015, **3**, 6286-6290.
- S. Roldán, C. Blanco, M. Granda, R. Menéndez and R. Santamaría, *Angew. Chem. Int. Ed.*, 2011, **50**, 1699-1701.
- S. T. Senthilkumar, R. K. Selvan, N. Ponpandian and J. S. Melo, *RSC Adv.*, 2012, **2**, 8937-8940.
- D. Vonlanthen, P. Lazarev, K. A. See, F. Wudl and A. J. Heeger, *Adv. Mater.*, 2014, **26**, 5095-5100.
- J. Q. Wei, H. W. Zhu, Y. H. Li, B. Chen, Y. Jia, K. L. Wang, Z. C. Wang, W. J. Liu, J. B. Luo, M. X. Zheng, D. H. Wu, Y. Q. Zhu and B. Q. Wei, *Adv. Mater.*, 2006, **18**, 1695-1700.
- S. Q. He, J. Q. Wei, F. M. Guo, R. Q. Xu, C. Li, X. Cui, H. W. Zhu, K. L. Wang, D. H. Wu, *J. Mater. Chem. A*, 2014, **2**, 5898-5902.
- R. Q. Xu, J. Q. Wei, F. M. Guo, X. Cui, T. Y. Zhang, H. W. Zhu, K. L. Wang and D. H. Wu, *RSC Adv.*, 2015, **5**, 22015-22021.
- H. J. Yu, J. H. Wu, L. Q. Fan, Y. Z. Lin, K. Q. Xu, Z. Y. Tang, C. X. Cheng, S. Tang, J. M. Lin, M. L. Huang and Z. Lan, *J. Power Sources*, 2012, **198**, 402-407.
- H. Y. Jin, L. M. Zhou, C. L. Mak, H. T. Huang, W. M. Tang, C. Wa and H. L. Han, *J. Mater. Chem. A*, 2015, **3**, 15633-15641.
- W. J. Liu, N. S. Liu, Y. L. Shi, Y. Chen, C. X. Yang, J. Y. Tao, S. L. Wang, Y. M. Wang, J. Su, L. Y. Li and Y. H. Gao, *J. Mater. Chem. A*, 2015, **3**, 13461-13467.
- Z. Y. Zhang, F. Xiao and S. Wang, *J. Mater. Chem. A*, 2015, **3**, 11215-11223.
- X. L. Zhao, B. N. Zheng, T. Q. Huang and C. Gao, *Nanoscale*, 2015, **7**, 9399-9404.
- Z. N. Yu and J. Thomas, *Adv. Mater.*, 2014, **26**, 4279-4285.
- P. Xu, T. Gu, Z. Y. Cao, B. Q. Wei, J. Y. Yu, F. Li, J. H. Byun, W. B. Lu, Q. W. Li and T. W. Chou, *Adv. Energy Mater.*, 2014, **4**, 1300759.
- J. Y. Tao, N. S. Liu, W. Z. Ma, L. W. Ding, L. Y. Li, J. Su and Y. H. Gao, *Sci. Rep.*, 2013, **3**, 2286.
- Q. H. Meng, H. P. Wu, Y. N. Meng, K. Xie, Z. X. Wei and Z. X. Guo, *Adv. Mater.*, 2014, **26**, 4100-4106.
- L. Kou, T. Q. Huang, B. N. Zheng, Y. Han, X. L. Zhao, K. Gopalsamy, H. Y. Sun and C. Gao, *Nat. Commun.*, 2014, **5**, 3754.
- J. Ren, W. Y. Bai, G. Z. Guan, Y. Zhang and H. S. Peng, *Adv. Mater.*, 2013, **25**, 5965-5970.
- Y. P. Fu, X. Cai, H. W. Wu, Z. B. Lv, S. C. Hou, M. Peng, X. Yu and D. C. Zou, *Adv. Mater.*, 2012, **24**, 5713-5718.
- J. R. Miller and P. Simon, *Science*, 2008, **321**, 651-652.

## Figures

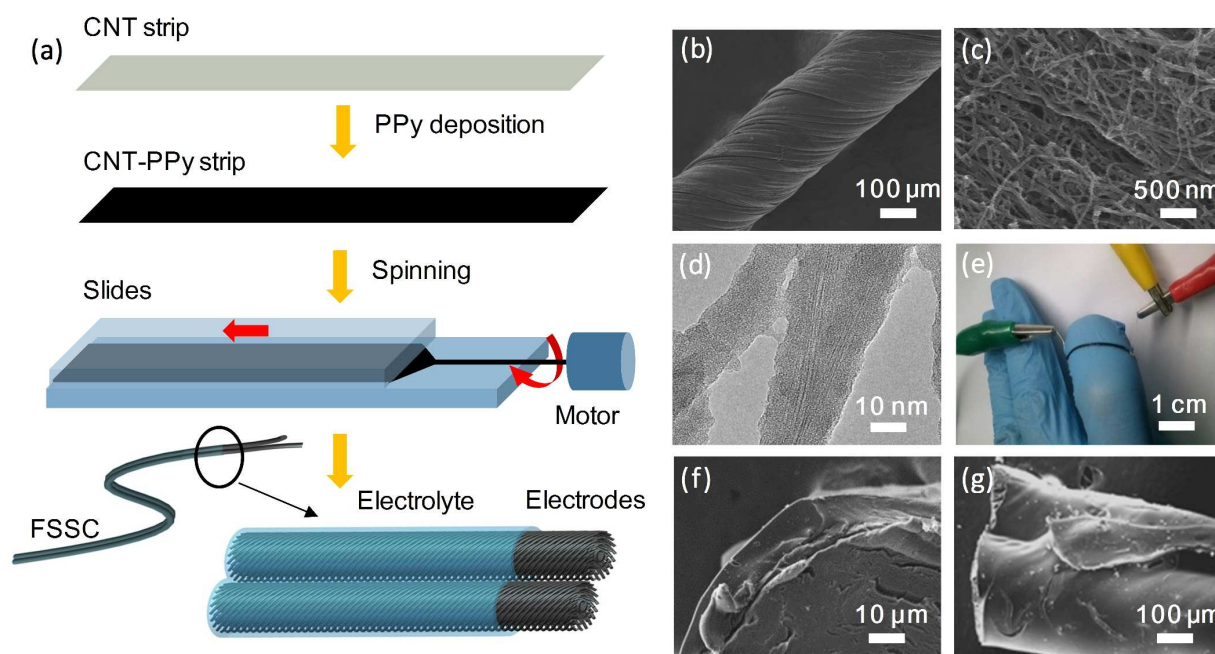


**Fig. 1** (a) Schematic illustration of the fabrication process of FSSCs. (b) Low magnification SEM image of a CNT-PPy fiber. (c) High magnification SEM image of a CNT-PPy fiber. (d) TEM image of the CNT-PPy nanocomposite. (e) Optical image of a FSSC wrapping on a finger. (f) Cross-sectional SEM image of a FSSC. (g) Side-viewed SEM image of a FSSC.

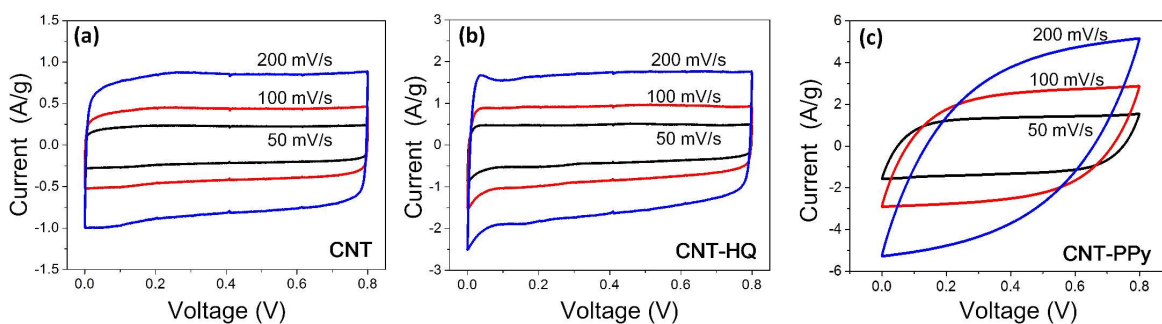


**Fig. 2** CV curves of the CNT-based FSSCs at various scan rates. (a) CNT, (b) CNT-HQ, (c) CNT-PPy.

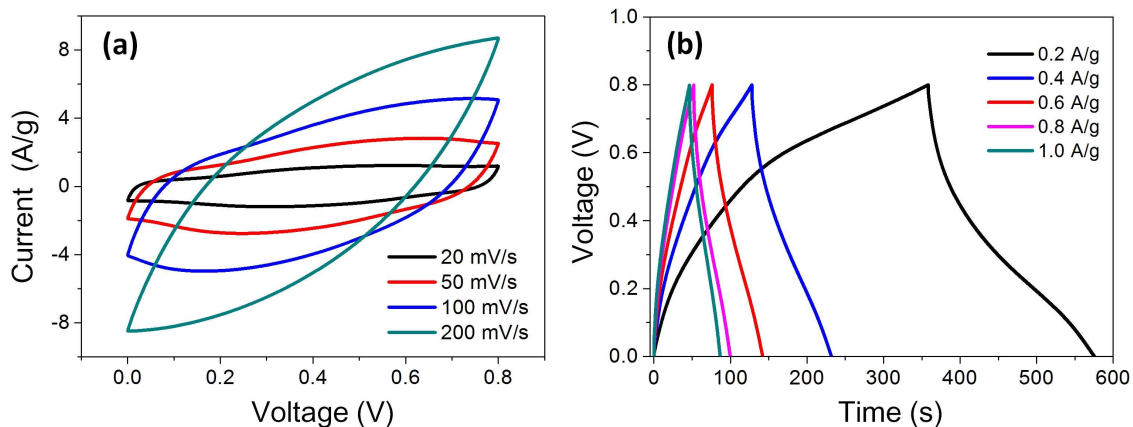


**Fig. 3** (a) CV curves and (b) GCD curves of a CNT-PPy-HQ FSSC at various scan rates and current densities.

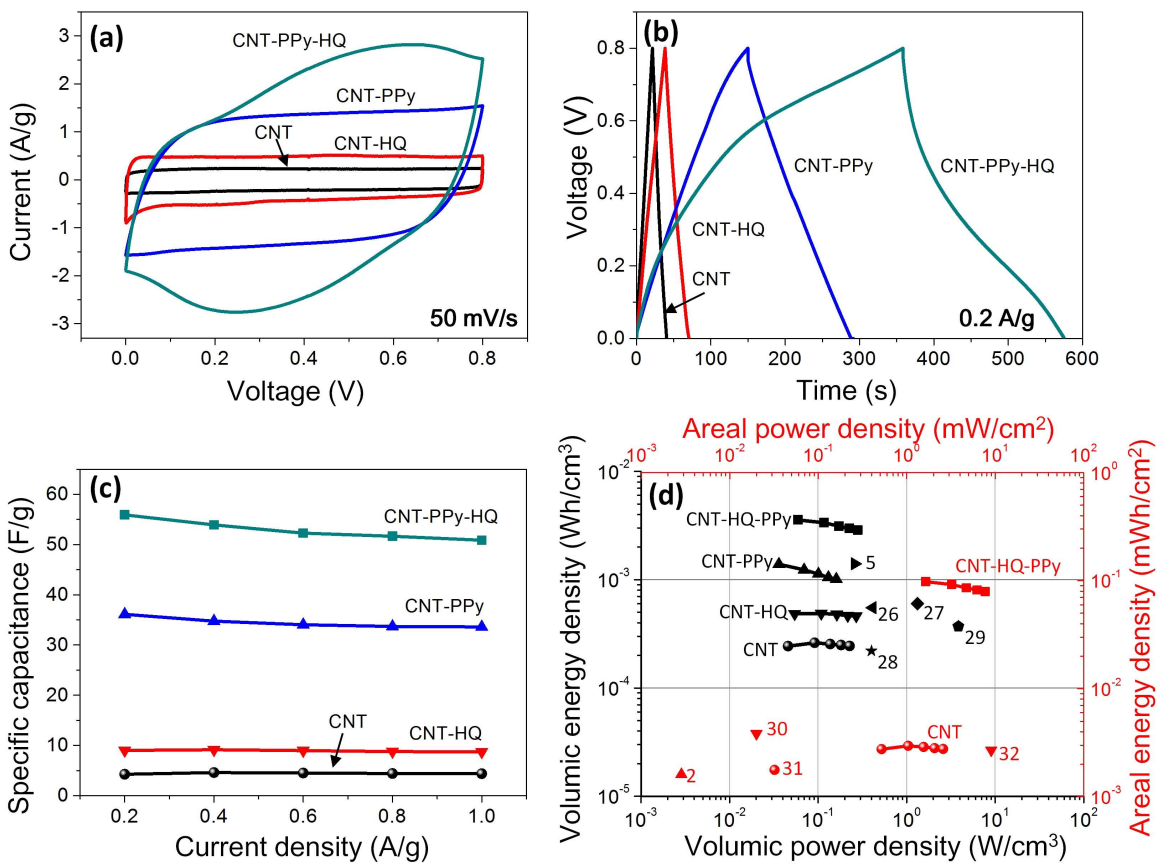


**Fig. 4** Comparison of the four kinds of FSSCs. (a) CV curves at 50 mV/s. (b) GCD curves at 0.2 A/g. (c) Plots of the specific capacitance vs. current density. (d) Ragone plots in terms of volume (black) and area (red).

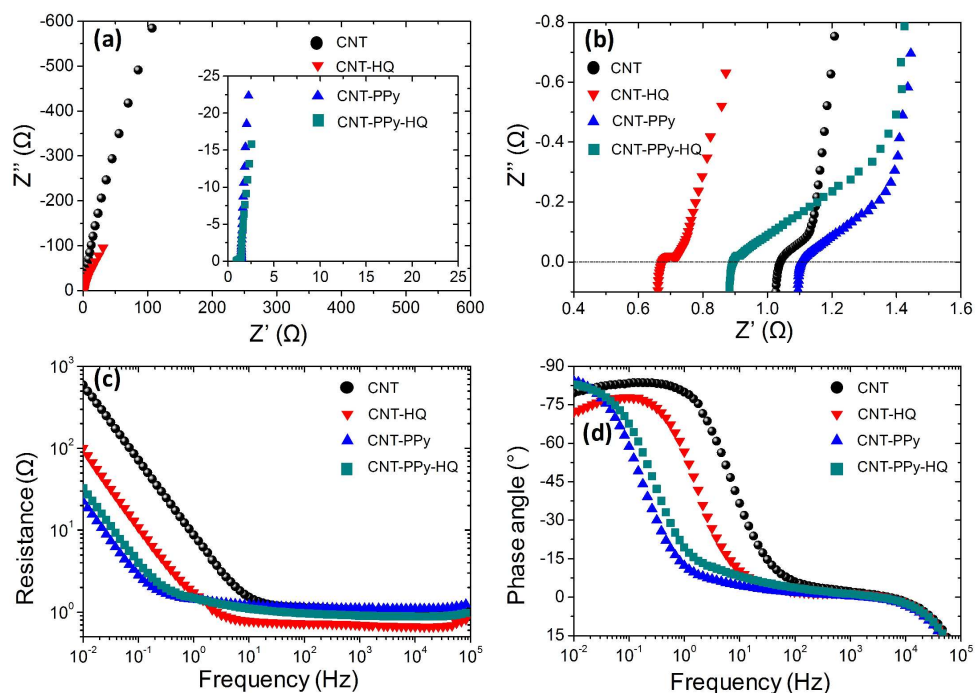


**Fig. 5** EIS analysis of the four kinds of FSSCs. (a) Nyquist plots. (b) Nyquist plots at high frequency region. (c) Frequency dependent resistances of Bode plots. (d) Frequency dependent phase angles of Bode plots.

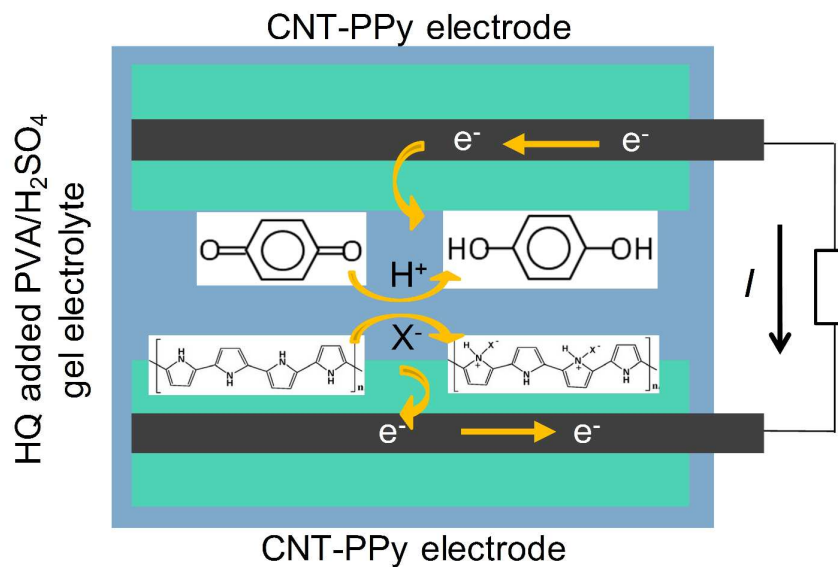


**Fig. 6** Schematic illustration of the working mechanism at the discharging process for the CNT-PPy-HQ FSSC.

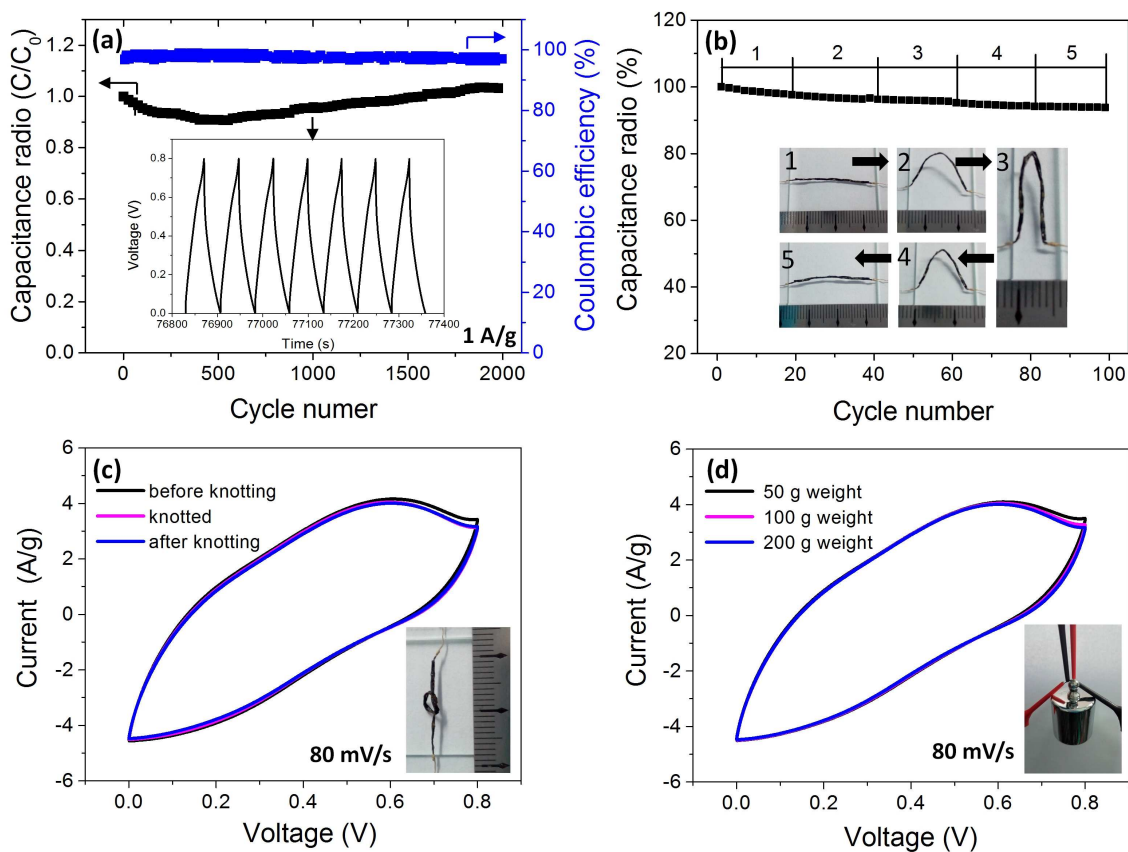


**Fig. 7** Stability and flexibility measurement of a CNT-PPy-HQ FSSC. (a) Capacitance retention of the FSSC during 2000 cyclic GCD test at 1 A/g. (b) Capacitance retention of the FSSC under bending and recovering. (c) CV curves of the FSSC being knotted. (d) CV curves of the FSSC hung with different weights.

## Graphical Abstract

A high performance fiber-shaped supercapacitor is fabricated from macroscopic CNT films by adding polypyrrole (PPy) to electrode and hydroquinone (HQ) to electrolyte, simultaneously. HQ and PPy have synergistic effects in the supercapacitor.

